Does shaping catalysts modify active phase sites? A comprehensive *in situ* FTIR spectroscopic study on the performance of a model Ru/Al_2O_3 catalyst for the CO methanation

L.F. Bobadilla, A. Muñoz-Murillo, O.H. Laguna, M.A. Centeno, J.A. Odriozola

PII: S1385-8947(18)31878-3
DOI: https://doi.org/10.1016/j.cej.2018.09.166
Reference: CEJ 20005

To appear in: *Chemical Engineering Journal*

Received Date: 21 April 2018
Revised Date: 11 September 2018
Accepted Date: 21 September 2018

Please cite this article as: L.F. Bobadilla, A. Muñoz-Murillo, O.H. Laguna, M.A. Centeno, J.A. Odriozola, Does shaping catalysts modify active phase sites? A comprehensive *in situ* FTIR spectroscopic study on the performance of a model Ru/Al_2O_3 catalyst for the CO methanation, *Chemical Engineering Journal* (2018), doi: https://doi.org/10.1016/j.cej.2018.09.166

Does shaping catalysts modify active phase sites? A comprehensive *in situ* FTIR spectroscopic study on the performance of a model Ru/Al_2O_3 catalyst for the CO methanation

L.F. Bobadilla*, A. Muñoz-Murillo, O.H. Laguna, M.A. Centeno and J.A. Odriozola

Instituto de Ciencia de Materiales de Sevila, Centro Mixto CSIC-Universidad de Sevilla, Av. Américo Vespucio 49, 41092 Sevilla (Spain)

(*) Corresponding author: bobadilla@icmse.csic.es (Luis F. Bobadilla)

Abstract

Routinely, it seems assumed that the catalytic layer coated on monoliths and microchannel reactors preserve the properties of the initial powder catalyst. However, this assumption should be reasonably demonstrated since the set of chemical and physical manipulations involved in the preparation of these catalytic devices hardly does not alter the surface of the starting catalyst powders. This work aims to evaluate the transformations that takes place in a model Ru/Al_2O_3 catalyst during a typical slurry preparation procedure and their impact on the catalytic performance for the CO methanation reaction and the selective methanation of CO in CO_2-rich reformate gases. For this purpose, we have conducted an *in situ* comprehensive study by means of Fourier Transform Infrared Spectroscopy (FTIR) in which the nature of the species present on the surface of the catalyst during CO hydrogenation was analyzed. This study reveals that during the preparation of the slurry the starting Ru/Al_2O_3 catalyst suffers a redispersion of metallic Ru particles and more surface hydroxyls are created by the incorporation of additional alumina. These modifications have a noticeable influence in the catalytic performance and despite their importance, these aspects have been poorly considered in other studies.

Keywords: *Ru catalyst; slurries preparation; CO methanation; in situ FTIR*

1. Introduction

CO methanation over different supported metal catalysts including Ni [1-3] , Ru [4, 5] and Rh [6, 7] has been widely investigated for the production of CH_4 from syngas and more recently also from a viewpoint of residual CO removal from H_2-rich feed gases for polymer electrolyte fuel cells (PEFCs) applications [8]. Because of the high CO_2 contents of typical reformate gases, catalysts for this application have to be extremely selective for CO methanation to avoid additional consumption of H_2 due to CO_2 methanation and reverse water gas shift (RWGS) reaction [9]. In this sense, ruthenium catalysts dispersed on metal oxide supports exhibit very high activity and selectivity for the selective methanation of CO [10]. CO methanation can be considered as a reaction model including various types of surface reactions (dissociation/recombination and hydrogenation/dehydrogenation reactions) as well as different sites of adsorption (step-edges and terraces). Higher activity of kinks and edges sites originates from dissociation of both H_2 and CO upon a single collision, whereas dissociation over more densely packed crystalline planes is much less probable [4].

The utilization of monoliths and microchannel-structured reactors with a thin layer of catalyst on the reactor channels walls have been proposed as an efficient alternative to the packed-bed catalysts in methanation reactions since heat and mass transport properties are strongly enhanced [8, 11-13]. Among the advantages of these catalytic systems over pellet catalysts, it is worth stressing the optimal reaction rates per mass unit of active-phase and the low-pressure drop working even at high flow rates [14]. However, the optimal performance of a monolithic catalyst depends on the formation of an adherent and uniform layer of catalyst on the microchannels.

The most widely used strategy to deposit a catalyst powder on a monolith substrate is the washcoating (or dip-coating) method in which a thin catalytic layer is formed [15]. The coated layer must be homogeneous with the desired catalyst

loading and proper adherence to the substrate. Moreover, the properties of the catalyst must be preserved: crystal structure, textural properties, acid-base and redox properties, and dispersion of the active phase. However, the monolith loading process involves physicochemical processes that may eventually modify the structure or the chemical composition of the initial catalyst powder, this modifying the catalytic performance. For instance, Hernández-Garrido et al. [16] evidenced that the spatial distribution of the different constituents of multicomponent catalysts based on ceria and the compositional features of the surface layer of the corresponding monoliths were significantly influenced by the washcoating process. They found that during the drying the suspension onto the monolith walls takes place an agglomeration of the ceria particles that subsequently affects to the catalytic performance. On the other hand, Germani et al. [17] reported that the addition of binders such as poly vinyl alcohol (PVA) on a Cu/Zn/Al catalyst decreases the surface area and deteriorates its catalytic in the water gas shift (WGS) reaction. They reported that binders that can form metal complexes must be avoided in order to prevent a redispersion of the active phase.

Therefore, the chemical and physical manipulations involved in the preparation of monolithic catalysts can modify the starting catalytic powders and to the best of our knowledge no so much attention has been paid in the study of the influence of the different steps of the preparation method on the final surface state of the monolith catalyst. In a previous work [18], we have reported that the structuration of a Ru/Al_2O_3 powder catalyst on stainless steel micromonoliths drives to more active and selective systems for CO methanation. The results obtained were ascribed to the metallic substrate, the presence of PVA and colloidal alumina in the slurry preparation as well as the aqueous acidic media and the thermal treatment used. In the current study, we have focused our efforts to investigate the transformations that may takes place in a model Ru/Al_2O_3 catalyst during the slurry preparation procedure and their impact on the catalytic performance for the CO methanation reaction. For this purpose, we have simulated a typical slurry preparation procedure

in which a suspension of the Ru/Al_2O_3 catalyst was stabilized in an aqueous solution that contains PVA and alumina colloidal as additives. This process may result in a partial reduction of the RuO_2 since PVA can as reducing agent and besides an additional amount of alumina can be incorporated to the catalytic formulation. To have more information on the surface chemistry of the initial powder catalyst and the surface state of the modified catalyst we have applied IR spectroscopic methods. Vibrational spectroscopic analysis with CO as probe molecule is a powerful method to study the interaction of the CO with the Ru metal particle and the surface hydroxyls as well as the subsequent reaction with hydrogen [19-22]. This investigation provides a better understanding of the surface modifications of the Ru/Al_2O_3 catalyst after adding additives and allows to deep on the CO methanation reaction. Finally, we have also analysed this effect in the catalytic performance for the methanation of residual CO in H_2-rich gas where CO_2 is also present.

2. Experimental procedure

2.1. Catalysts preparation

The catalyst was prepared by using the wet impregnation method. For it, a commercial γ-Al_2O_3 support (Sasol, Puralox Scca 30/100) was impregnated with the adequate amount of ruthenium (III) nitrosyl nitrate solution (Johnson Matthey) diluted in water (200 ml per gram of support) in order to obtain a theoretical Ru loading of 10 wt.%. After 15 min stirring at room temperature the solvent was removed on rotavapor and the obtained solid was dried at 130 °C overnight and finally calcined at 400 °C for 2h.

In order to investigate the effect of binders (alumina) and dispersants/protective agents (polyvinyl alcohol, PVA) involved in the preparation of slurries we have prepared a powder representative of the final washcoated. For this purpose, the adequate amount of Ru/Al_2O_3 was dispersed in deionised water and stabilized with polyvinyl alcohol (PVA), and subsequently the commercial γ-Al_2O_3 (Sasol, Puralox Scca 30/100) was added using a proportion equal to 1:15 (wt/wt) of alumina:catalyst.

Afterwards, the mixture was kept for 48 h under vigorous stirring. Finally, the solid was dried at 130 °C for 24 h and calcined at 400 °C for 2 h obtaining a "physical-mixture" Ru/Al_2O_3-Alumina that can be representative of the final state of the catalyst layer in a monolith.

2.2. Characterization methods

The chemical composition of the catalyst prepared was estimated by X-Ray fluoresecence (XRF) using a Panalytical AXIOS PW4400 spectrometer with a rhodium tube as source.

X-ray diffraction (XRD) analysis was performed on an X'Pert Pro PANalytical instrument. Diffraction patterns were recorded using Cu Kα radiation (λ=1.5418 Å, 40 mA and 45 kV) over a 2θ-range of 10–90° and a position-sensitive detector using a step size of 0.05° and a step time of 80 s.

Temperature-programmed reduction (TPR) experiments were carried out in a conventional apparatus in which a quartz reactor is connected to a TCD detector minimizing the volume of the tubing between the reactor and the detector to minimize the relaxation time of the temperature measurement. A stream of 5 vol.% H_2 in Ar with a flow rate of 50 mL min^{-1} was passed through a bed of 50 mg of sample, and the temperature was increased linearly at a heating rate of 10 °C min^{-1} from room temperature to 400 °C. A solid CO_2-acetone trap was used to condense the reduction products, mainly water. Quantitative analyses were performed by integration of the reduction signal and comparison with hydrogen consumption of a CuO reference sample.

Transmission electron microscopy (TEM) micrographs were obtained in a Phillips CM 200 working at 200 kV with EDS analysis and CCD camera. The powder samples were previously dispersed in ethanol absolute by ultrasonication and supported in a hollowed carbon coated cupper grid (Lacey Carbon Film, 300 mesh copper grid).

2.3. *In situ* FTIR spectroscopic experiments

The IR spectra were recorded in transmission mode on a Thermo Nicolet Avatar 380 FTIR spectrometer equipped with a DTGS/KBr detector and accumulating 128 scans with a resolution of 4 cm^{-1}. The sample powder was pressed into self-supporting pellets of ca. 20 mg cm^{-2} and treated directly in a homemade IR cell. The material window used is CaF_2 that only allows access to wavenumber ranges above 1000 cm^{-1}. The cell is connected to a vacuum line with a residual vacuum below 10^{-5} mbar. This cell setup allows treatments under static conditions up to pressures of 200 mbar and the temperature is controlled by a thermocouple placed close to the pellet. Prior to the measurements, the sample wafer was reduced by heating for 1 h in hydrogen (120 mbar) at 300 °C and 30 minutes of evacuation in vacuum at the same temperature. After pretreatment, the sample was exposed to small doses of CO (4 mbar) up to saturation at room temperature and then evacuated in vacuum also at the same temperature to remove the CO weakly adsorbed. Subsequently, a pressure of 66 mbar of hydrogen was added and the temperature was increased at intervals of 50 °C up to 300 °C to investigate the evolution of the surface species on the catalyst and the products formed in gas phase. All surface spectra were corrected with the spectrum of the sample after reduction pretreatment prior to adsorption.

2.4. CO selective methanation activity measurements

Selective CO methanation catalytic activity was evaluated in a Microactivity PID Eng&Tech equipment using a tubular AISI316 stainless steel reactor (9 mm i.d.). The powder samples (140 mg sieved in the 100-200 μm range) were diluted in a volume of 7.5 cm^3 of glass balls of the same diameter. A mixture of H_2 (50%), CO_2 (15%), H_2O (15%), CO (0.03 %) and N_2 balanced was used simulating the real products from the outlet stream of a CO preferential oxidation (PROX) reaction unit with a WHSV (Weight Hourly Space Velocity) fixed at 80 L g^{-1} min^{-1}. Prior to reaction, the catalysts were activated at 300 $^{\circ}C$ for 2 h under continuous flow rate of 60 mL min^{-1} of pure H_2 and then the temperature was

adjusted at 110 °C in 60 mL min^{-1} of pure N_2. The reaction was performed at temperatures between 110 °C and 280 °C. The conversion curves were obtained by analyzing on-line the concentration of CO and CO_2, where the CO is followed by a microGC Varian 4900 and the CO_2 is determined by a CO_2 detector Vaisala CARBOCAP GMT220.

3. Results and discussion

3.1. Structure and reducibility of the catalysts

The chemical analysis by XRF spectrometry reveals that the real Ru loading in the prepared catalyst was 8.6 wt.%. By using this measured value, we estimated that the Ru/Al_2O_3 and Ru/Al_2O_3-alumina samples contain 0.86 and 0.80 mmol of Ru for 1 g of sample, respectively.

Figure 1 shows XRD patterns of Ru/Al_2O_3 and Ru/Al_2O_3-alumina catalysts before and after reduction. The diffraction peaks obtained can be assigned to the following phases: γ-Al_2O_3 (JCPDS 46-1215) and RuO_2 (JCPDS 40-1290). It should be noted that the crystalline structure of the bare catalyst remains unchanged in spite of the addition of alumina. From the broadening of the reflection peak of the (110) plane at 28° and applying the Scherrer equation, the mean crystallite sizes of RuO_2 particles were estimated to be ca. 8.5 and 9 nm for Ru/Al_2O_3 and Ru/Al_2O_3-alumina catalysts, respectively. Additionally, both samples were pretreated at 300 °C for 2h in H_2 and RuO_2 phase is fully reduced to metallic Ru (JCPDS 06-0663, Fig. 1) and the estimated particle size of Ru from the (101) plane at 44.01° resulted to be 7.2 and 6.5 nm for Ru/Al_2O_3 and Ru/Al_2O_3-alumina catalysts, respectively.

Insert here Fig.1

The reducibility of Ru/Al_2O_3 and Ru/Al_2O_3-alumina catalysts was studied by temperature-programmed reduction. TPR profiles of both samples are shown in Figure 2. The occurrence of only one reduction peak in both cases is directly ascribed to the total reduction of RuO_2 to Ru^0 since it is supposed that the ruthenium oxide is the only specie to be reduced [23, 24]. As can be observed, the presence of additional alumina on the

Ru/Al_2O_3 catalyst resulted in significant modification of the reducibility in which the peak maximum was displaced from 225 °C to 197 °C. This suggests that the catalyst have been slightly modified during the preparation of the simulated slurry suffering a possible redispersion of metallic Ru particles. This better dispersion simultaneously with the alumina presence enhance significantly the reducibility of the Ru/Al_2O_3 catalyst. This proposition is in agreement with the results obtained by *in situ* FTIR spectroscopic studies as will be discussed with more detail in the following section.

Insert here Fig.2

3.2. *In situ* FTIR spectroscopic studies

3.2.1. CO adsorption

Carbon monoxide was introduced, at room temperature, into the IR cell under static conditions by adding successive aliquots of 4 mbar. After every addition an IR spectrum was recorded. Fig. 3 shows the series of IR spectra obtained after CO exposure. For clarity, difference spectra are shown. The IR spectra hardly change after the successive CO exposures in the 1200-1800 cm^{-1} region being dominated by bands at 1654, 1480, 1437 and 1237 cm^{-1} ascribed to bicarbonate species as early proposed by Morterra et al. [25]. Besides these bands a set of absorptions in the 1800-2200 cm^{-1} region assigned to adsorbed carbonyl species appears. Upon CO_2 adsorption on γ-Al_2O_3, Vimont et al. [26] assigned bands at 1648, 1485, and 1234 cm^{-1} to adsorbed bicarbonate species, and Szanyi and Kwak. [27] also assigned features appearing at 1230, 1437, 1480 and 1654 cm^{-1} to B1 and B2 type bicarbonate species adsorbed on γ-Al_2O_3. The bands at *ca.* 1650 and 1230 cm^{-1} appear at similar positions for both types of bicarbonates being only noticeable a shift of 8 and 5 cm^{-1}, respectively, close to our spectral resolution, when B1 bicarbonates are transformed into the B2 ones. The bands at 1480 and 1437 cm^{-1} are assigned to the O-C-O symmetric stretching mode in B2 and B1 bicarbonate species, respectively [25]. Szanyi and Kwak [27] proposed that the key difference between B1 and B2 species does not depend on the nature of the bicarbonate but on the interaction of the alumina hydroxyls groups with the bicarbonates species. For these authors, B2 bicarbonates are only formed

on highly dehydroxylated alumina surfaces, which is in accordance with Morterra et al. [25] that points to the presence of structural defects on the alumina surface for generating B2 bicarbonates. Recently, Jimenez-Barrera et al. [28] has observed the presence of an isosbestic point that evidences the reversible interconversion of B2 and B1 species. This interconversion is related to the degree of hydroxylation of the alumina surface that is also related to surface defects as proposed by Morterra et al. [29]. It should be noticed that a band at 2360 cm^{-1} characteristic of CO_2 weakly interacting with coordinatively unsaturated tetrahedral Al^{3+} sites [29] appears in the physical mixture but is absent in the Ru/Al_2O_3 catalyst. This reveals that the amount of structural defects on the alumina is higher in the physical mixture as will be discussed below. The B2:B1 $\nu(OCO)_s$ mode intensity ratio is 0.69 and 0.97 for the Ru/Al_2O_3 catalyst and the Ru/Al_2O_3-Al_2O_3 physical mixture, respectively. This modification of the intensity ratio suggests that the alumina addition has modified the number of surface defects that implies a surface reconstruction of the γ-Al_2O_3 support. An analysis of the hydroxyl stretching region confirms this suggestion. Bands in the OH stretching region are clearly modified upon CO adsorption, difference spectra accounting for band intensity modification in this region upon CO adsorption.

Insert here Fig.3

From a crystallographic point of view, the γ-Al_2O_3 support may be described as a defective spinel containing both tetrahedral and octahedral Al^{3+} cations. However, the existence of defects induces the presence of under coordinated cations, which results in almost amorphous surface containing an enormous variety of coordination environments for the Al^{3+} cations [30, 31]. According to Onfroy et al. [32], the band at 3760-3780 cm^{-1} is ascribed to type I terminal hydroxyl (Al_{5c}) and those at 3730-3735 and 3700-3710 cm^{-1} are attributed to type II bridging hydroxyl ($Al_{5c}Al_{3c}$)OH and type III triply bonded hydroxyl $(Al_{5c})_3OH$, respectively. The intensity decrease observed in figure 3 must be related to the formation of B2 bicarbonates that growth at the expenses of type I terminal hydroxyl (Al_{5c}) hydroxyls with the participation of type III triply bonded hydroxyl $(Al_{5c})_3OH$. Besides these modifications, a band at 3610 cm^{-1} ascribed ν(OH) in adsorbed bicarbonate species

appears [25, 33]. Hydroxyl bands are hardly noticeable in the Ru/Al_2O_3 catalyst that on the other hand is the sample that present a lesser amount of the B2 bicarbonates. Carbonates are formed upon CO_2 interaction with the support surface. Several possibilities may be envisaged for the production of CO_2 as reflected in the following equations:

$$CO + 2 * \longrightarrow C^* + O^* \qquad (Eq.1)$$

$$CO + O^* \longrightarrow CO_2 + * \qquad (Eq.2)$$

$$CO + * \longrightarrow CO^* \qquad (Eq.3)$$

$$CO^* + Al - OH \longrightarrow HOCO^* + Al_{cus} \qquad (Eq.4)$$

$$HOCO^* \longrightarrow CO_2 + \frac{1}{2}H_2 + * \qquad (Eq.5)$$

where (*) stands for a Ru site and Al_{cus} for an Al cation associated to an oxygen vacancy. The Boudouard reaction on Ru particles (Eq. 1 and 2), may account for the formation of CO_2. At temperatures above 150 °C this reaction takes place on Ru/Al_2O_3 catalysts [28]. Moreover, it has been found that a small amount of Ru on Ni/Al_2O_3 catalysts may favor CO disproportion [34], which is in accordance with early studies on the interaction of CO with single crystal Ru surfaces [35]. The interaction of adsorbed CO on Ru sites with OH groups of the support [36] may result in the formation of adsorbed carboxyl species that are known to be a key intermediate in the WGS reaction (eq. 4 and 5) [37]. The excellent activity of Ru-based catalysts in the WGS reaction may support this hypothesis [38]. However, the small changes observed in the OH stretching region, hardly noticeable in the Ru/Al_2O_3 catalyst, suggest hydroxyl groups of the support are mainly involved in the formation of bicarbonates through their interaction with the CO_2 formed via CO disproportionation on Ru sites. Nevertheless, CO reaction with hydroxyls groups of the support cannot be disregarded as a pathway for carbonate formation. It is worth mentioning that the development of the B2 type bicarbonate species is favored in the sample based on the physical mixture although the amount of B1 species is very similar in both samples.

Fig. 4 shows the CO stretching vibrational region in detail. A weak feature is observed at 2175 cm^{-1}, and although CO adsorbed at low temperature on Lewis acidic sites located on low index crystal planes of the alumina support may result in a band at this frequency [29], the extremely low thermal stability of these species allows discarding their presence in our experimental conditions. Moreover, the R and P branches of gas-phase CO appear at *ca.* 2170 and 2115 cm^{-1} being the intensity of the former higher than that of the later, this suggests that the very weak feature at 2175 cm^{-1} accounts for the presence of residual gas phase CO.

Insert here Fig.4

At high CO coverages the spectrum of both the Ru/Al_2O_3 catalyst and the Ru/Al_2O_3-Al_2O_3 physical mixture are dominated by a band peaking at 2049 cm^{-1} assigned to CO linearly adsorbed on metallic Ru sites. Bands at this frequency have been observed for CO adsorption on Ru(0001) single crystal surfaces and on supported Ru clusters [39]. In general, large terraces are required for observing this band since this adsorption occurs in high coordinated Ru sites. At low CO coverages significant differences between both samples are noticed. After the introduction of the first dose (Fig. 4 inlet), the spectra of both samples present the same set of bands peaking at 2129, 2068, 2049 and 2025 cm^{-1} but their relative intensity depends on the sample. In his pioneering work on CO adsorption on Ru/Al_2O_3 catalysts, Dalla-Beta [40] established a correlation between the Ru particle size and the stretching frequency of the adsorbed CO bonds, in such a way that on increasing the particle size a red shift is observed for the CO stretching frequency. For particles with an average size of 1.3 nm the linear CO adsorbed on Ru sites appears at 2050 cm^{-1} while for bigger particles particles the stretching mode undergoes a red shift appearing at 2028 cm^{-1} for ~10 nm particles. Chin et al. [41] synthesized Ru particles in the 1.2-1.5 nm range and on these particles they found a band upon CO adsorption at 2038 cm^{-1} that they ascribed to linear CO adsorbed on Ru^0 sites [42]. However, these authors do not observe any shift on sintering the Ru nanoparticles but a collection of different sites indicating that a band at 2015 cm^{-1} may account for linearly adsorbed CO on high energy defect sites and/or

isolated Ru^0 species surrounded by partially oxidized Ru, [Ru^0-CO]. Dulaurent et al. [43] observed a shift of the 2047 cm^{-1} band to 2020 cm^{-1} upon carbon deposition as a result of CO disproportionation. A similar assignment has been proposed by Hadjiivanov et al. [21] although these authors indicate that this band may be also ascribed to ruthenium dicarbonyl species. Combining IR, NMR and DFT, Comes-Vives et al. [44] studied the nature of the CO adsorbed species on Ru nanoparticles and they found for metallic nanoparticles in the 1.4-1.6 nm range a collection of absorption bands between 2013 and 2082 cm^{-1} that they assign to different types of linearly adsorbed CO species.

Insert here Table 1

Furthermore, the band at 2129 cm^{-1} may be ascribed to multicarbonyl species. According to Chin et al. [42] this band indicates the existence of oxidized ruthenium sites, i.e. $Ru^{\delta+}(CO)_x$. This assignment is in agreement with early studies by several authors on Ru supported on different oxides [19, 20, 45]. Hadjiivanov et al. [21] comprehensively details the observed frequency values for multicarbonyl Ru species on different supports, Table 1. Although only metallic Ru should be expected on the catalyst surface after the high temperature reduction pretreatment (figure 2) the high capacity of metallic Ru to dissociate CO into adsorbed C* and O* species should result in Ru partially oxidized, although this hypothesis is not generally accepted [21, 46]. However, the evolution of CO_2 resulting in bicarbonate species support the CO dissociation and hence the presence of residual carbon deposits on the Ru surface and the presence of the weak band at 2360 cm^{-1} that indicates the existence of weakly adsorbed CO_2 on the support. The presence of germinal CO groups in small Ru particles (average particle sizes below 6 nm) has also been proposed as responsible of the 2129 cm^{-1} band [39]. Solymosi et al. [19] found that the hydroxyl groups of the alumina may be involved in the formation of Ru polycarbonyl species and molecular hydrogen according to the reaction (Eq. 6):

$$Ru^0 + 2Al - OH + xCO \longrightarrow (AlO)_2Ru^{\delta+}(CO)_x + H_2 \qquad (Eq.6)$$

Evidences for the occurrence of this interaction may rely on the intensity decrease of the v(OH) at 3790 cm^{-1} associated to isolated Al-OH groups observed upon CO adsorption (see

Fig. 3). However, bicarbonate formation also occurs at the expenses of these hydroxyls and the very small intensity decrease observed should account for both bicarbonate formation and the CO-induced oxidative disruption of the Ru nanoparticles.

Several conclusions may be drawn from the relative intensity of adsorbed CO bands in the studied samples. First, it may be assumed that a wide size distribution of Ru nanoparticles is obtained following our preparation method and hence that the differences in the relative intensity of the bands at 2049 and 2025 cm^{-1} in Ru/Al_2O_3 and Ru/Al_2O_3-Al_2O_3 catalysts may be related to differences in Ru particle size. Thus the higher the intensity ratio between the 2025 and 2049 cm^{-1} bands the bigger the average particle size of Ru nanoparticles. Moreover, on decreasing the Ru particle size the formation of gem-dicarbonyl species either on oxidized Ru sites [21] or at set edges of very small Ru particles is favored [39]. This again suggest that the average particle size of the Ru/Al_2O_3-Al_2O_3 catalyst is smaller that of the Ru/Al_2O one.

By plotting the intensity of the adsorbed carbonyl bands against the amount of CO added to the IR cell the metal dispersion can be estimated, figure 5. The intensity of the adsorbed CO band should increase linearly up to the monolayer capacity and further on remain constant for increased amounts of CO admitted into the IR cell. For both studied samples the monolayer capacity occurs for the same amount of CO admitted into the IR cell, ~$9 \cdot 10^{17}$ molecules, and considering that the amount of Ru is the same in both samples the metal dispersion should be the same and estimate at *ca*. 11%. Considering an average particle size of 8.5-9 nm as deduced from Scherrer analysis of the XRD pattern a dispersion of 14-15% is estimated in close agreement with the CO adsorption data [47]. However, the area under the CO adsorption curve is lower by ~20% in the Ru/Al_2O_3-Al_2O_3 sample than in the Ru/Al_2O_3 catalyst. This should indicate either that the extinction molar coefficient for CO has changed, which did not seem feasible, or that a part of the CO molecules reacts with the metal surface resulting in adsorbed species different of CO. Apart from the CO the only observable adsorbed species are bicarbonates but the IR bands characteristics of these species show intensities quite similar for both samples ruling out

these species as responsible for the observed differences in figure 5. Therefore, the observed difference may account for carbon species left behind upon CO dissociation on Ru sites. The smaller the metallic particles the higher the dissociation probability at step or corner sites upon adsorption resulting in adsorbed carbon that may reduce the average number of adsorbed CO molecules.

Insert here Fig.5

Therefore, it may be claimed that in the process of adding the alumina excess the Ru particle size distribution is modified. Figure 6 shows the TEM images of both the Ru/Al_2O_3-Al_2O_3 and the Ru/Al_2O_3 catalysts in both cases a wide particular size distribution is observed but on adding the alumina the average particle size shifts to lower values. The average particle size, d_{av}, was estimated through equation 7 considering the relative contribution of the particles of different sizes (d_i):

$$d_{av} = \frac{\sum n_i d_i^3}{\sum n_i d_i^2} \qquad (\text{Eq. } 7)$$

The estimate d_{av} values are 8.2 and 6.6 nm for Ru/Al_2O_3 and Ru/Al_2O_3-Al_2O_3 catalysts, respectively. Moreover, it should be noted in the particle size distribution (Fig. 6) that the proportion of smaller particles (between 3 and 4 nm) is superior in the Ru/Al_2O_3-Alumina catalyst as illustrate the schematic representation. The average particle size decrease may be associated to the slurry preparation procedure, the stabilization of the Ru/Al_2O_3-Al_2O_3 catalyst implies the catalyst suspension in a water PVA-solution that is further heated for 24 hours at 130°C under continuous stirring for completely evaporating the liquid. This process may result in a partial reduction of the RuO_2 nanoparticles since polyvinyl alcohol (PVA), like other capping molecules, may act as steric stabilizer but also as reducing agent, for instance it has been used for reducing Pd salts and stabilizing the obtained nanoparticles [48]. Although it is known that dissolution of the crystalline phase of RuO_2 is difficult [49], a modification in the oxidation state of the metal by removing oxygen atoms from the structure induces oxide dissolution [50]. This reduction-dissolution process results in the

observed modification of the particle size distribution and hence on the CO adsorption changes observed.

Insert here Fig.6

3.2.2. CO methanation

Once the surface species after CO saturation and evacuation at RT were stabilized, hydrogen was introduced into the IR cell (66 mbar) and the temperature was increased stepwise each 50 °C up to 300 °C. Figure 7 shows the evolution of the surface species during the evacuation and the hydrogenation in function of the temperature. During the evacuation step at RT, the only change observed was the disappearance of the bands at 2360 and 2175 cm^{-1}. As we mentioned above, these bands are associated to CO_2 physisorbed linearly on alumina sites and CO adsorbed on Al^{3+} Lewis acid sites, respectively. Both species are weakly adsorbed and become removed at RT. The other adsorbed species remains mostly intact upon evacuation at room temperature. On the other hand, it is clearly evidenced that upon hydrogen introduction in the cell at RT, the band at 2129 cm^{-1} disappeared completely. In presence of hydrogen, the $Ru^{\delta+}$ multicarbonyl species formed during the oxidative disruption process are reduced towards H-assisted paths resulting small Ru^0 clusters that subsequently may agglomerate to larger Ru clusters **[51]**. The corresponding linearly bonded CO species exhibits moderate stability at low temperatures. Nevertheless, its concentration, and consequently, the intensity of the band centered at 2050 cm^{-1} decreases rapidly when the temperature is increased. Besides, the analysis of the gas phase shows the formation of methane (Fig. 7 inset) indicating that the CO hydrogenation is taking place. It should be noted that even at high temperatures a band at 1950 cm^{-1} still remain. A similar feature was observed by Wasylenko and Frei [52] for CO hydrogenation at elevated temperatures as a result of the decreasing surface concentration of CO. It has been proposed that this band at 1950 cm^{-1} is characteristic of bridge-bonded CO on Ru zerovalent sites with a slightly different energy and could be attributed to the decrease in the CO surface coverage, which allows the transformation of some linearly to bridged bonded sites at higher temperatures [42]. This suggest that CO

diadsorbed on two Ru sites does not enter into the reaction of methanation in concordance with the results previously reported [53, 54]. Simultaneously, it is worth noting that under hydrogen atmosphere the bands associated to bicarbonates species also undergo significant changes. As shown Fig. 7, the disappearance of B2 type bicarbonate is much faster than that of B1 bicarbonate species which still remain on the surface at 100 °C. As we have mentioned above, the B2 type of bicarbonates are formed on defective Al sites of partially dehydroxylated alumina. The earlier disappearance suggests that hydrogen inhibits these defects and B2 type species are converted into B1 type species. The IR features developed at 1370, 1390 and 1590 cm^{-1}, which are characteristic of adsorbed formate species [55], are formed by reduction of bicarbonates, and taking into account that the dissociation of hydrogen occurs on the Ru sites, it can expected that this reaction occur at the interface of Ru sites and alumina support.

Insert here Fig.7

Evolution of both B1 and B2 types of bicarbonates as well as formates, represented by the band height at 1437, 1480 and 1590 cm^{-1}, respectively, are shown in Fig. 8. It is clearly evidenced that B2 type carbonates are converted into B1 type bicarbonates, and formates are formed at expenses of these ones. Solymosi et al. [19] reported that most of the formates formed are migrated from the metal/oxide interface to the support. The formate species are only reactive toward the formation of CO adsorbed whether are close to the metallic sites. However, the migration to the metal/oxide interface is energetically unfavored and requires high temperatures [56]. We believe that formate species are not involved in the CO methanation and remain on the support like spectators, although may also play a role in agreement with Garbarino et al. [57]. It must not be discarded the presence of water generated by the reaction between the hydrogen and the O* created upon CO dissociation over Ru surface sites. In fact, we observed changes in the bands of the hydroxyls although because of the lack of spectral resolution this region is not showed.

Insert here Fig.8

Fig. 9 shows the evolution of the methane formed in gas phase and the disappearance of the IR absorption band area for adsorbed CO species (2100-2000 cm^{-1}) It can be appreciated that exists a direct correlation between the methane formation and the linearly CO adsorbed species disappearance. Kobori et al. [46] reported that the hydrogenation of CO to form methane and longer hydrocarbons proceeds on Ru metallic sites via the carbon formed by dissociative adsorption of CO. Methane is formed via further hydrogenation of carbon species like C* and CH_x* and subsequent desorption. Wasylenko and Frei [52] demonstrated that the linearly CO adsorbed on Ru sites are the kinetically most relevant centers for the rate-determining CO dissociation step. Other authors [39] proposed that the CO hydrogenation involves the formation of formyl species (HCO*) followed by the irreversible reaction of HCO* and H* to form hydroxymethylene (HCOH*), which dissociates into CH* and OH*.

Insert here Fig.9

Comparing the results obtained on both Ru/Al_2O_3 catalysts, it is clear that during the slurry preparation procedure takes place modifications on the catalyst surface that enhances the catalyst performance towards the formation of methane. We attribute this observation mainly to the presence of additional hydroxyl groups that favor the oxidative disruption of Ru-Ru bonds leading to a reconstruction of the surface of the ruthenium particles. These particles favor the dissociation/disproportionation of CO leading to adsorbed carbon that is selectively hydrogenated to methane. This is in line with the results reported by Kwak et al. [58], which reveal that methane formation is selectively favored after the formation of 3D metal clusters on a Ru/Al_2O_3 catalyst. They suggest that Ru clusters exhibit a good catalytic activitiy toward CH_4 formation above a certain cluster size whereas single Ru atoms or interfacial Ru favor CO formation. This can be explained by the fact that the competition between hydrogen and CO is limited to certain sites, i.e. it is a structure-sensitive reaction. By means of density functional theory (DFT) calculations and IR spectroscopy, Lovelless et al. [39] demonstrated that H-assisted CO activation is more favored on terraces sites of Ru than in low-coordination environments like corner and edge

sites suggesting that these sites are less reactive. It is therefore necessary to obtain particles with an optimal size to favor the methanation of CO. We have observed that the isolated OH groups on the alumina are involved in the formation of Ru multicarbonyl species by oxidative disruption process. The presence of hydrogen causes the reductive agglomeration of $Ru^{\delta+}$ sites and subsequently takes place a surface structural reorganization of the particles generating Ru clusters that are very active for the methane formation. This small clusters favor the dissociation of hydrogen and are able to supply large amount of H* species for the CO hydrogenation step. The results obtained show that linear carbonyl species are the main intermediate involved in the CO methanation and the reaction proceeds via hydrogenation of surface carbon produced by CO adsorption dissociative on metal Ru particles with the optimal size.

3.3. Catalytic performance on CO selective methanation

The methanation selective of CO was evaluated in both samples at temperatures between 100 and 280 °C. Fig. 10 shows the CO and CO_2 conversions plotted as functions of the reaction temperature. It can be observed that CO conversion increases with increasing temperature and reaches 100 % at 150 °C for the Ru/Al_2O_3 – alumina catalyst whereas the Ru/Al_2O_3 catalyst goes through a maximum at ca. 90% at 220 °C. At temperatures above 220 °C, both catalysts are active for the reverse water gas shift (RWGS) reaction increasing the CO_2 conversion and the rate of CO production becomes equilibrated with the rate of CO consumption via methanation reaction [10]. Furthermore, at higher temperatures the CO_2 methanation reaction becomes important. Panagiotopoulou et al. [59] reported that methanation of CO occurs via two distinct reaction pathways. The first one takes place at lower temperatures and involves the hydrogenation of surface carbon produced by dissociative adsorption of CO, whereas the second occurs at higher temperatures under conditions of CO_2 methanation and proceeds with intermediate formation of Ru_x-CO species at the metal−support interface via the RWGS reaction. In the selective methanation of CO in CO/CO_2 mixtures, the conversion of CO_2 is suppressed because of the kinetically faster hydrogenation of surface carbon, which is produced

dissociative adsorption of CO on Ru sites. This is concordance with our observations by FTIR CO adsorption.

Insert here Fig.10

The differences observed in the catalytic performance on CO selective methanation can be ascribed to the influence of the additives used in the slurry preparation method. As we have demonstrated above, the presence of PVA and alumina colloidal provokes a surface structural reorganization of the particles generating Ru clusters that are very active for the methane formation. The population of these species increases significantly with increasing the population of hydroxyl. This better dispersion simultaneously with the alumina presence enhance the reducibility of the Ru/Al_2O_3 catalyst as was demonstrated by TPR measurements. Therefore, our results clearly indicate the monolith layer catalyst hardly preserve the structure of the starting catalyst powders and such changes affect notably to the catalytic performance.

4. Conclusions

The present work was focused on the study of the structural modifications that takes place in a model Ru/Al_2O_3 catalyst during the slurry preparation procedure and their impact on the catalytic performance for the CO methanation reaction and the selective methanation of CO in CO_2-rich reformate gases. It was clearly demonstrated that the modifications suffered in the catalyst surface affect notably the catalytic behavior enhancing the activity. It was found that the average size of Ru particles in the Ru/Al_2O_3-Al_2O_3 catalyst is smaller that of the Ru/Al_2O_3 one. This indicates that during the preparation of the slurry the starting Ru/Al_2O_3 catalyst suffers a redispersion of metallic Ru particles. The presence of PVA and alumina colloidal provokes a surface structural reorganization of the particles generating Ru clusters that are very active for the methane formation. Besides more surface hydroxyls are created by the incorporation of additional alumina. From a mechanistic point of view, it is observed that CO species linearly bonded on reduced Ru crystallites are the active species in the CO methanation reaction whereas that formate species likely are not involved in the reaction and remain on the support like spectators. Therefore, this study highlights that the

deposition of the stabilized catalyst suspension onto the monolith walls hardly preserve the structural properties of the starting catalyst powders. This approach offers a new perspective that should be considered in the study of the catalytic performance for monolith catalysts and microchannels reactors.

Acknowledgments

Financial support for this work has been obtained from the Spanish Ministerio de Economía y Competitividad – MINECO (ENE2015-66975-C3-2-R) co-financed by FEDER funds from the European Union. Luis F. Bobadilla thanks MINECO for the Juan de la Cierva Incorporación 2015 contract.

References

[1] T.A. Le, M.S. Kim, S.H. Lee, T.W. Kim, E.D. Park, CO and CO_2 methanation over supported Ni catalysts, Catal. Today 293-294 (2017) 89-96.

[2] J. Sehested, S. Dahl, J. Jacobsen, J.R. Rostrup-Nielsen, Methanation of CO over Nickel: Mechanism and kinetics at high H_2/CO ratios, J. Phys. Chem. B 109 (2005) 2432-2438.

[3] M.P. Andersson, F. Abild-Pedersen, I.N. Remediakis, T. Bligaard, G. Jones, J. Engbæk, O. Lytken, S. Horch, J.H. Nielsen, J. Sehested, J.R. Rostrup-Nielsen, J.K. Nørskov, I. Chorkendorff, Structure sensitivity of the methanation reaction: H_2-induced CO dissociation on nickel surfaces, J. Catal. 255 (2008) 6-19.

[4] P. Djinović, C. Galletti, S. Specchia, V. Specchia, CO methanation over Ru–Al_2O_3 catalysts: Effects of chloride doping on reaction activity and selectivity, Top. Catal. 54 (2011) 1042.

[5] S. Tada, R. Kikuchi, K. Urasaki, S. Satokawa, Effect of reduction pretreatment and support materials on selective CO methanation over supported Ru catalysts, Appl. Catal. A Gen. 404 (2011) 149-154.

[6] B.A. Sexton, G.A. Somorjai, The hydrogenation of CO and CO_2 over polycrystalline rhodium: Correlation of surface composition, kinetics and product distributions, J. Catal. 46 (1977) 167-189.

[7] R.W. McCabe, R.K. Usmen, K. Ober, H.S. Gandhi, The effect of alumina phase-structure on the dispersion of rhodium/alumina catalysts, J. Catal. 151 (1995) 385-393.

[8] C. Galletti, S. Specchia, V. Specchia, CO selective methanation in H_2-rich gas for fuel cell application: Microchannel reactor performance with Ru-based catalysts, Chem. Eng. J. 167 (2011) 616-621.

[9] R.A. Dagle, Y. Wang, G.-G. Xia, J.J. Strohm, J. Holladay, D.R. Palo, Selective CO methanation catalysts for fuel processing applications, Appl. Catal. A Gen. 326 (2007) 213-218.

[10] A.M. Abdel-Mageed, D. Widmann, S.E. Olesen, I. Chorkendorff, J. Biskupek, R.J. Behm, Selective CO methanation on Ru/TiO_2 Catalysts: Role and influence of metal–support interactions, ACS Catal. 5 (2015) 6753-6763.

[11] S. Danaci, L. Protasova, J. Lefevere, L. Bedel, R. Guilet, P. Marty, Efficient CO_2 methanation over Ni/Al_2O_3 coated structured catalysts, Catal. Today 273 (2016) 234-243.

[12] K.P. Brooks, J. Hu, H. Zhu, R.J. Kee, Methanation of carbon dioxide by hydrogen reduction using the Sabatier process in microchannel reactors, Chem. Eng. Sci. 62 (2007) 1161-1170.

[13] V. Meille, Review on methods to deposit catalysts on structured surfaces, Appl. Catal. A Gen. 315 (2006) 1-17.

[14] O.H. Laguna, M.I. Domínguez, M.A. Centeno, J.A. Odriozola, Chapter 4 - Catalysts on metallic surfaces: Monoliths and microreactors, in: New Materials for Catalytic Applications, Elsevier, Amsterdam, 2016, pp. 81-120.

[15] X. Xiaoding, H. Vonk, A. Cybulski, J.A. Moulijn, Alumina washcoating and metal deposition of ceramic monoliths, in: G. Poncelet, J. Martens, B. Delmon, P.A. Jacobs, P. Grange (Eds.) Stud. Surf. Sci. Catal., Elsevier, 1995, pp. 1069-1078.

[16] J.C. Hernández-Garrido, D.M. Gómez, D. Gaona, H. Vidal, J.M. Gatica, O. Sanz, J.M. Rebled, F. Peiró, J.J. Calvino, Combined (S)TEM-FIB insight into the influence of the preparation method on the final surface structure of a Co_3O_4/La-modified-CeO_2 washcoated monolithic catalyst, J. Phys. Chem. C 117 (2013) 13028-13036.

[17] G. Germani, A. Stefanescu, Y. Schuurman, A.C. van Veen, Preparation and characterization of porous alumina-based catalyst coatings in microchannels, Chem. Eng. Sci. 62 (2007) 5084-5091.

[18] A. Muñoz-Murillo, L.M. Martínez T, M.I. Domínguez, J.A. Odriozola, M.A. Centeno, Selective CO methanation with structured RuO_2/Al_2O_3 catalysts, Appl. Catal. B Environ. 236 (2018) 420-427.

[19] F. Solymosi, J. Raskó, An infrared study of the influence of CO adsorption on the topology of supported ruthenium, J. Catal. 115 (1989) 107-119.

[20] M. Kantcheva, S. Sayan, On the mechanism of CO adsorption on a silica-supported ruthenium catalyst, Catal. Lett. 60 (1999) 27-38.

[21] K. Hadjiivanov, J.C. Lavalley, J. Lamotte, F. Maugé, J. Saint-Just, M. Che, FTIR study of CO interaction with Ru/TiO_2 catalysts, J. Catal. 176 (1998) 415-425.

[22] T. Mizushima, K. Tohji, Y. Udagawa, A. Ueno, An EXAFS and IR study of the CO adsorption-induced morphology change in ruthenium catalysts, J. Am. Chem. Soc. 112 (1990) 7887-7893.

[23] P. Betancourt, A. Rives, R. Hubaut, C.E. Scott, J. Goldwasser, A study of the ruthenium–alumina system, Appl. Catal. A Gen. 170 (1998) 307-314.

[24] I. Balint, A. Miyazaki, K.-i. Aika, The relevance of Ru nanoparticles morphology and oxidation state to the partial oxidation of methane, J. Catal. 220 (2003) 74-83.

[25] C. Morterra, A. Zecchina, S. Coluccia, A. Chiorino, IR spectroscopic study of CO_2 adsorption onto η-Al_2O_3, J. Chem. Soc. Faraday Trans. 73 (1977) 1544-1560.

[26] A. Vimont, J.C. Lavalley, A. Sahibed-Dine, C. Otero Areán, M. Rodríguez Delgado, M. Daturi, Infrared spectroscopic study on the surface properties of γ-gallium oxide as compared to those of γ-alumina, J. Phys. Chem. B 109 (2005) 9656-9664.

[27] J. Szanyi, J.H. Kwak, Dissecting the steps of CO_2 reduction: 1. The interaction of CO and CO_2 with [gamma]-Al_2O_3: an in situ FTIR study, Phys. Chem. Chem. Phys. 16 (2014) 15117-15125.

[28] E. Jiménez-Barrera, P. Bazin, C. López-Cartes, F. Romero-Sarria, M. Daturi, J.A. Odriozola, CO/H_2 adsorption on a Ru/Al_2O_3 model catalyst for Fischer Trospch: Effect of water concentration on the surface species, Appl. Catal. B Environ. 237 (2018) 986-995.

[29] C. Morterra, G. Magnacca, A case study: surface chemistry and surface structure of catalytic aluminas as studied by vibrational spectroscopy of adsorbed species, Catal. Today 27 (1996) 497-532.

[30] L.J. Álvarez, J.F. Sanz, M.J. Capitán, M.A. Centeno, J.A. Odriozola, Surface models for [gamma]-Al_2O_3 from molecular dynamics simulations, J. Chem. Soc. Faraday Trans. 89 (1993) 3623-3628.

[31] L.J. Álvarez, L.E. Leon, J.F. Sanz, M.J. Capitán, J.A. Odriozola, Computer simulation of gamma-Al_2O_3 microcrystal, J. Phys. Chem. 99 (1995) 17872-17876.

[32] T. Onfroy, W.-C. Li, F. Schuth, H. Knözinger, Surface chemistry of carbon-templated mesoporous aluminas, Phys. Chem. Chem. Phys. 11 (2009) 3671-3679.

[33] J. Baltrusaitis, J.H. Jensen, V.H. Grassian, FTIR spectroscopy combined with isotope labeling and quantum chemical calculations to investigate adsorbed bicarbonate formation following reaction of carbon dioxide with surface hydroxyl groups on Fe_2O_3 and Al_2O_3, J. Phys. Chem. B 110 (2006) 12005-12016.

[34] A. Álvarez M, M.Á. Centeno, J.A. Odriozola, Ru–Ni catalyst in the combined dry-steam reforming of methane: The importance in the metal order addition, Top. Catal. 59 (2016) 303-313.

[35] E. Shincho, C. Egawa, S. Naito, K. Tamaru, The behaviour of CO adsorbed on Ru(1,1,10) and Ru(001); the dissociation of CO at the step sites of the Ru(1,1,10) surface, Surf. Sci. 149 (1985) 1-16.

[36] K. Föttinger, R. Schlögl, G. Rupprechter, The mechanism of carbonate formation on Pd-Al_2O_3 catalysts, Chem. Commun. (2008) 320-322.

[37] S.D. Senanayake, D. Stacchiola, P. Liu, C.B. Mullins, J. Hrbek, J.A. Rodriguez, Interaction of CO with OH on Au(111): HCOO, CO_3, and HOCO as key intermediates in the water-gas shift reaction, J. Phys.Chem. C 113 (2009) 19536-19544.

[38] W. Xu, R. Si, S.D. Senanayake, J. Llorca, H. Idriss, D. Stacchiola, J.C. Hanson, J.A. Rodriguez, In situ studies of CeO_2-supported Pt, Ru, and Pt–Ru alloy catalysts for the water–gas shift reaction: Active phases and reaction intermediates, J. Catal. 291 (2012) 117-126.

[39] B.T. Loveless, C. Buda, M. Neurock, E. Iglesia, CO chemisorption and dissociation at high coverages during CO hydrogenation on Ru catalysts, J. Am. Chem. Soc. 135 (2013) 6107-6121.

[40] R.A. Dalla-Betta, Carbon monoxide adsorption on supported ruthenium, J. Phys. Chem. 79 (1975) 2519-2525.

[41] S.Y. Chin, O.S. Alexeev, M.D. Amiridis, Preferential oxidation of CO under excess H_2 conditions over Ru catalysts, Appl. Catal. A Gen. 286 (2005) 157-166.

[42] S.Y. Chin, C.T. Williams, M.D. Amiridis, FTIR studies of CO adsorption on Al_2O_3- and SiO_2-supported Ru catalysts, J. Phys. Chem. B 110 (2006) 871-882.

[43] O. Dulaurent, M. Nawdali, A. Bourane, D. Bianchi, Heat of adsorption of carbon monoxide on a Ru/Al_2O_3 catalyst using adsorption equilibrium conditions at high temperatures, Appl. Catal. A Gen. 201 (2000) 271-279.

[44] A. Comas-Vives, K. Furman, D. Gajan, M.C. Akatay, A. Lesage, F.H. Ribeiro, C. Coperet, Predictive morphology, stoichiometry and structure of surface species in supported Ru nanoparticles under H_2 and CO atmospheres from combined experimental and DFT studies, Phys. Chem. Chem. Phys. 18 (2016) 1969-1979.

[45] J.L. Robbins, Chemistry of supported Ru: CO-induced oxidation of Ru at 310 K, J. Catal. 115 (1989) 120-131.

[46] Y. Kobori, S. Naito, T. Onishi, K. Tamaru, H_2-D_2 kinetic isotope effect in CO hydrogenation over Ru/SiO_2, J. Chem. Soc. Chem. Commun. (1981) 92-93.

[47] G. Bergeret, P. Gallezot, Handbook of Heterogeneous Catalysis, 2nd ed., Wiley VCH Verlag 1998.

[48] W. Hoogsteen, L.G.J. Fokkink, Polymer-Stabilized Pd Sols: Kinetics of sol formation and stabilization .echanism, J. Colloid Interface Sci. 175 (1995) 12-26.

[49] Y. Lee, J. Suntivich, K.J. May, E.E. Perry, Y. Shao-Horn, Synthesis and activities of rutile IrO_2 and RuO_2 nanoparticles for oxygen evolution in acid and alkaline solutions, J. Phys. Chem. Lett. 3 (2012) 399-404.

[50] N. Hodnik, P. Jovanovič, A. Pavlišič, B. Jozinović, M. Zorko, M. Bele, V.S. Šelih, M. Šala, S. Hočevar, M. Gaberšček, New insights into corrosion of ruthenium and ruthenium Oxide nanoparticles in acidic media, J. Phys. Chem. C 119 (2015) 10140-10147.

[51] A.M. Abdel-Mageed, S. Eckle, D. Widmann, R.J. Behm, Water assisted dispersion of Ru nanoparticles: The impact of water on the activity and selectivity of supported Ru catalysts during the selective methanation of CO in CO_2-rich reformate, J. Catal. 335 (2016) 79-94.

[52] W. Wasylenko, H. Frei, Direct observation of the kinetically relevant site of CO hydrogenation on supported Ru catalyst at 700 K by time-resolved FT-IR spectroscopy, Phys. Chem. Chem. Phys. 9 (2007) 5497-5502.

[53] C.S. Kellner, A.T. Bell, Infrared studies of carbon monoxide hydrogenation over alumina-supported ruthenium, J. Catal. 71 (1981) 296-307.

[54] M. Nawdali, H. Ahlafi, G.M. Pajonk, D. Bianchi, Elementary steps involved in the hydrogenation of the linear CO species adsorbed on a Ru/Al_2O_3 catalyst, J. Mol. Catal. A Chem. 162 (2000) 247-256.

[55] J.M. Trillo, G. Munuera, J.M. Criado, Catalytic decomposition of formic acid on metal oxides, Catal. Rev. 7 (1972) 51-86.

[56] X. Wang, Y. Hong, H. Shi, J. Szanyi, Kinetic modeling and transient DRIFTS–MS studies of CO_2 methanation over Ru/Al_2O_3 catalysts, J. Catal. 343 (2016) 185-195.

[57] G. Garbarino, D. Bellotti, E. Finocchio, L. Magistri, G. Busca, Methanation of carbon dioxide on Ru/Al_2O_3: Catalytic activity and infrared study, Catal. Today 277 (2016) 21-28.

[58] J.H. Kwak, L. Kovarik, J. Szanyi, CO_2 reduction on supported Ru/Al_2O_3 catalysts: Cluster size dependence of product selectivity, ACS Catal. 3 (2013) 2449-2455.

[59] P. Panagiotopoulou, D.I. Kondarides, X.E. Verykios, Selective methanation of CO over supported Ru catalysts, Appl. Catal. B Environ. 88 (2009) 470-478.

LIST OF FIGURES AND TABLES

Table 1. Assignments proposed by Hadjiivanov et al. [21] for high frequency bands after CO adsorption on supported Ru/Al_2O_3 catalysts

Figure 1. XRD pattern of both fresh and reduced catalysts: (A) Ru/Al_2O_3, and (B) Ru/Al_2O_3-Alumina

Figure 2. TPR-profile of both samples

Figure 3. FTIR spectra collected after adsorption of small doses of CO (4 mbar) at room temperature for both catalysts

Figure 4. FTIR spectra collected after adsorption of small doses of CO (4 mbar) at room temperature for both catalysts in the spectral range 1900-2500 cm^{-1}

Figure 5. Plot of adsorbed CO band intensity versus the amount of CO admitted into the IR cell for both samples

Figure 6. TEM micrographs and particle size distribution

Figure 7. FTIR spectra obtained during the evacuation and the hydrogenation in function of the temperature for both samples. Inset: evolution of methane formed in gas phase

Figure 8. Evolution of the band height at 1437, 1480 and 1590 cm^{-1}, associated to B1 and B2 type bicarbonates and formates, respectively, in function of the temperature

Figure 9. Evolution of the band area of methane in gas phase and carbonyls region in function of the temperature

Figure 10. Catalytic activity of both catalysts for the selective CO methanation. Reaction conditions: H_2 (50%), CO_2 (15%), H_2O (15%), CO (0.03%) balanced in N_2, WHSV = 80 L g^{-1} min^{-1}. The samples were pretreated at 300 ^{o}C for 2 h in 60 mL min^{-1} of hydrogen

Table 1.

Species	**Frequencies / cm^{-1}**
$[Ru^{2+}(CO)_3]$	2112, 2072
$[Ru^{\partial+}(CO)_3]$	2140, 2072
$[Ru^{3+}(CO)_2]$	2138, 2070-2075
$[Ru^{3+}(CO)_2]$	2083-2075, 2029-2025
$[Ru^{\partial+}(CO)_2]$	2070–50, 2002–1970
$Ru^{\partial+}(CO)_2]$; $3 \geq \delta \geq 1$	2140, 2075

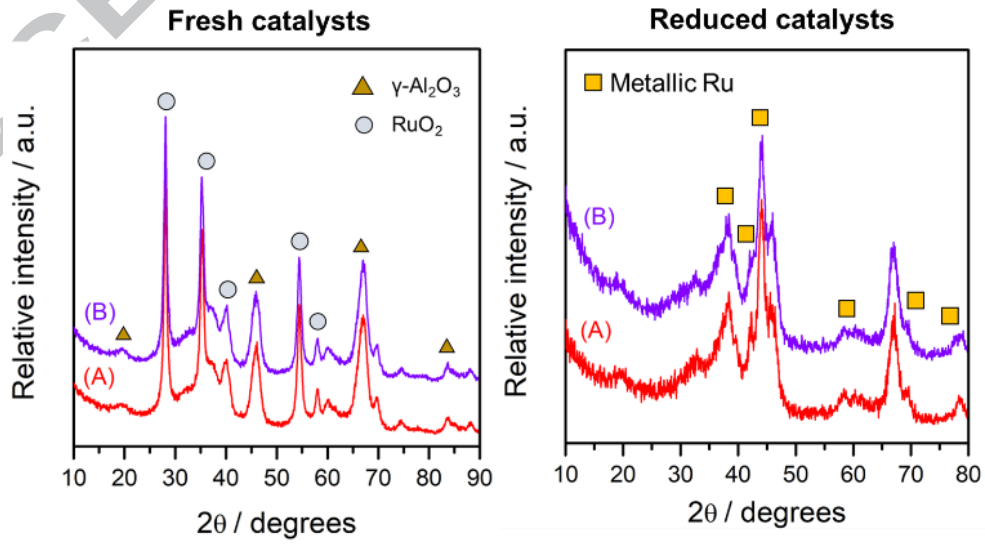

Figure 1.

Figure 2.

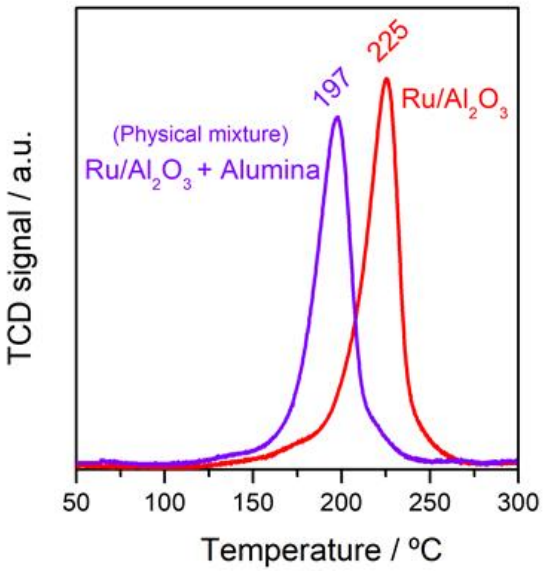

Figure 3.

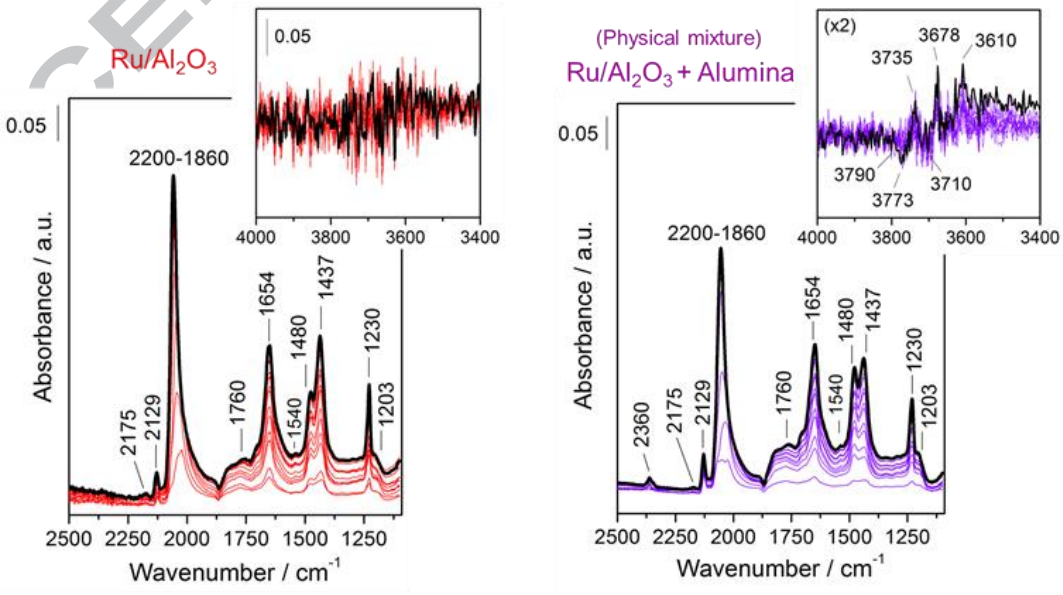

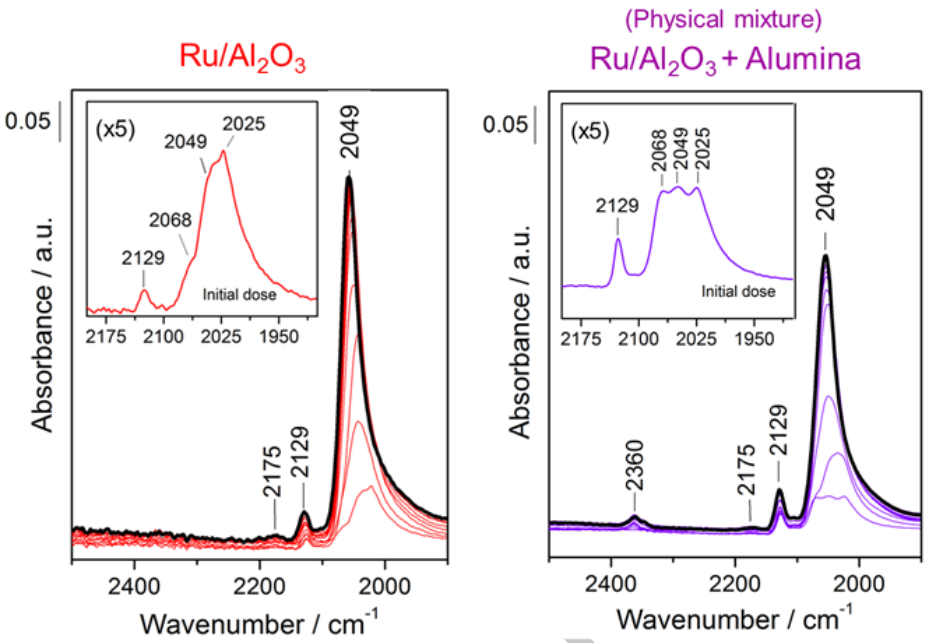

Figure 4.

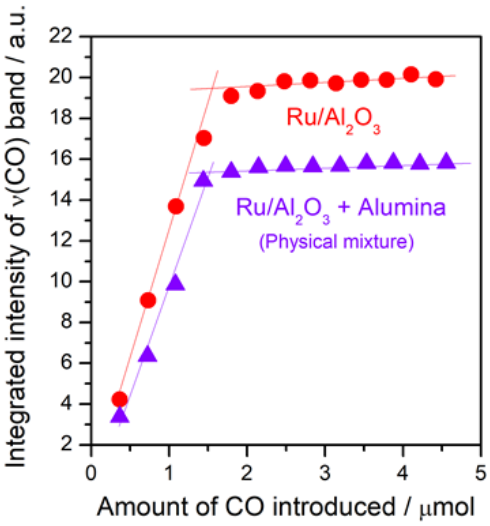

Figure 5.

Figure 6.

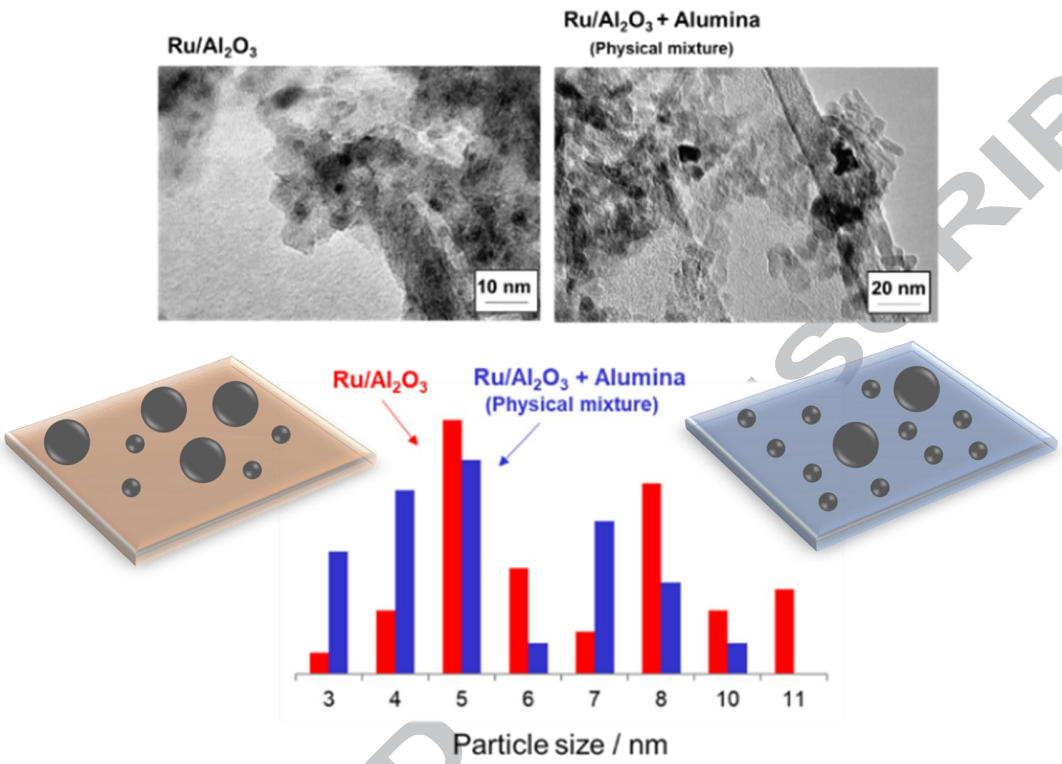

Figure 7.

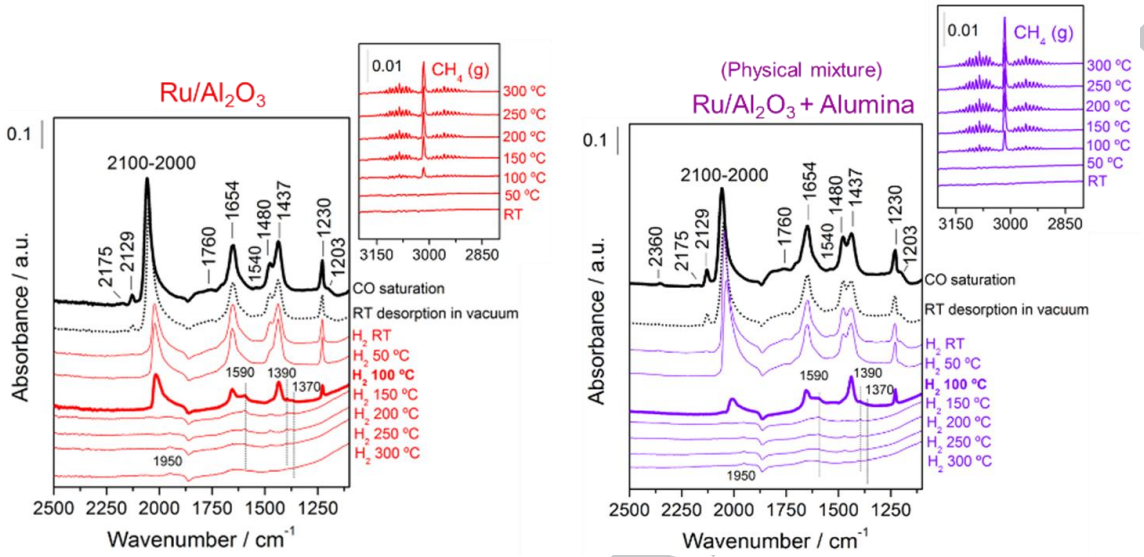

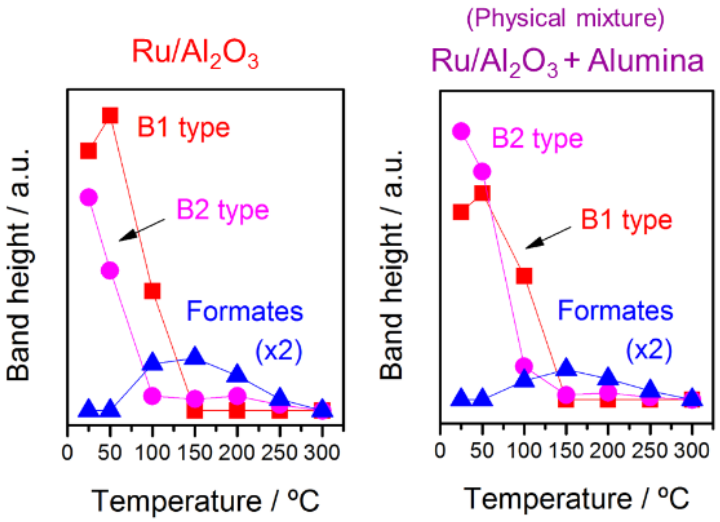

Figure 8.

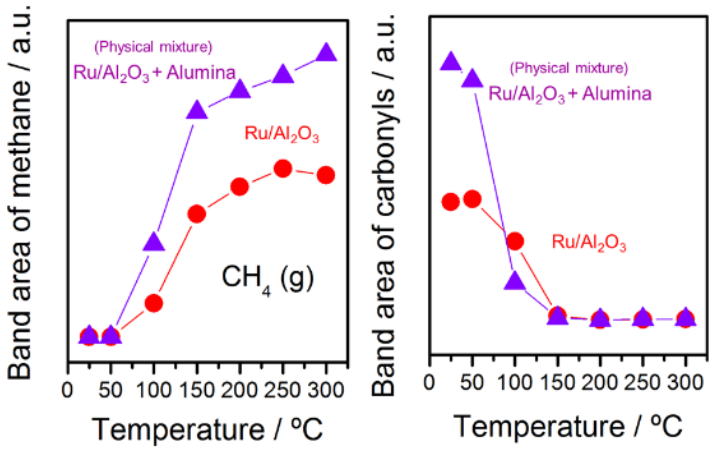

Figure 9.

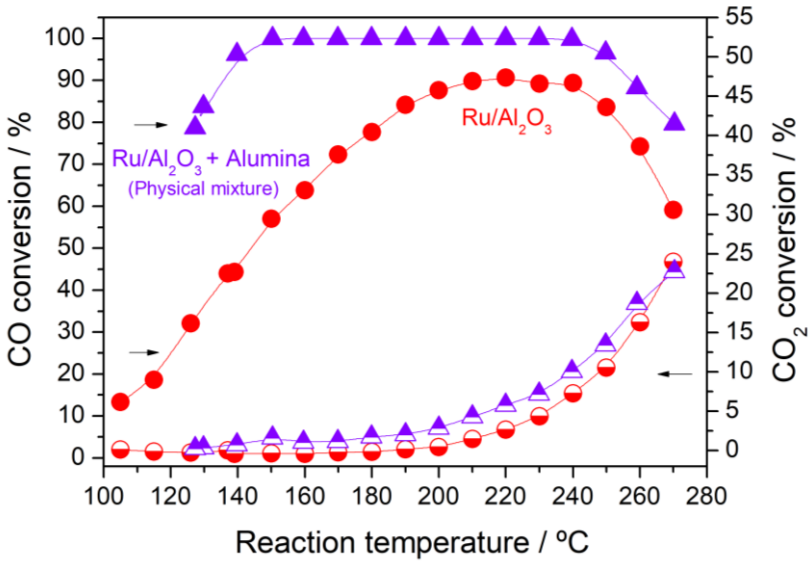

Figure 10.

Highlights

- ✓ Structural modifications take place in the catalyst during the slurry preparation
- ✓ The presence of additives provokes a surface structural reorganization generating Ru clusters very active
- ✓ CO species linearly bonded on reduced Ru crystallites are the active species in the CO methanation